JGR Atmospheres

RESEARCH ARTICLE
10.1029/2020JD032710

Key Points:
- CRTM simulation is found to underestimate CrIS shortwave infrared LTE and NLTE radiances
- A new statistical method is developed to quantify NLTE effects from CrIS FSR radiance observations in both daytime and nighttime
- The new method is complementary to existing RTM NLTE simulation and can help improve the applications of NLTE-affected radiances

Correspondence to:
Z. Li,
zhenglong.li@ssec.wisc.edu

Citation:
Li, Z., Menzel, W. P., Jung, J., Lim, A., Li, J., Matricardi, M., et al. (2020). Improving the understanding of CrIS full spectral resolution nonlocal thermodynamic equilibrium radiances using spectral correlation. *Journal of Geophysical Research: Atmospheres*, *125*, e2020JD032710. https://doi.org/10.1029/2020JD032710

Received 5 MAR 2020
Accepted 29 JUN 2020
Accepted article online 25 JUL 2020

Improving the Understanding of CrIS Full Spectral Resolution Nonlocal Thermodynamic Equilibrium Radiances Using Spectral Correlation

Zhenglong Li[1], W. Paul Menzel[1], James Jung[1], Agnes Lim[1], Jun Li[1], Marco Matricardi[2], Manuel López-Puertas[3], Sergio DeSouza-Machado[4], and L. Larrabee Strow[4,5]

[1]Cooperative Institute for Meteorological Satellite Studies, University of Wisconsin-Madison, Madison, WI, USA, [2]ECMWF, Reading, UK, [3]Instituto de Astrofisica de Andalucia, CSIC, Granada, Spain, [4]Joint Center for Earth Systems Technology, University of Maryland, Baltimore County, Baltimore, MD, USA, [5]Department of Physics, University of Maryland, Baltimore County, Baltimore, MD, USA

Abstract In recent years, significant progress has been made in fast radiative transfer model (RTM) simulation of daytime nonlocal thermodynamic equilibrium (NLTE) emission. However, NLTE remains as one important reason that prevents the hyperspectral shortwave infrared (SWIR) radiance observations from being assimilated into numerical weather prediction (NWP) models. To better understand the limitations of existing RTM-based NLTE simulation, this study introduces a new statistical method, called Spectral Correlations to Estimate Non-Local Thermal Equilibrium (SCENTE), to estimate the NLTE radiances in the Cross-track Infrared Sounder (CrIS) SWIR radiance observations. SCENTE is applied to four typical season days, including spring equinox, summer solstice, fall equinox, and winter solstice. By analyzing calculation/background minus observation (BMO) of CrIS SWIR brightness temperature (BT), results show that SCENTE characterizes the NLTE well with standard deviation of differences (STD) comparable to observation noise for both daytime and nighttime, while the community RTM (CRTM) has substantially larger STD at night, mainly due to the lack of daytime NLTE just beyond the day/night terminator and the lack of aurora-related NLTE. Detailed investigation of the biases of BMO shows that CRTM underestimates daytime SWIR NLTE effects by 0.76 K, while SCENTE overestimates SWIR NLTE effects by 0.70 K. The overestimation is because SCENTE uses CRTM-simulated SWIR local thermodynamic equilibrium (LTE) radiances in the training, which is underestimated by 0.70 K in BT. SCENTE, complementary to RTM-based simulations, can be used for quality control of SWIR radiances for assimilation and retrieval of atmospheric soundings.

1. Introduction

Hyperspectral Infrared (HIR) sounders (Menzel et al., 2018), such as Atmospheric InfraRed Sounder (AIRS), Infrared Atmospheric Sounding Interferometer (IASI), and Cross-track Infrared Sounder (CrIS), provide useful thermodynamic information for global numerical weather prediction (NWP) models, especially the sounding channels around the 15 μm CO_2 absorption band. Studies have shown that HIR sounders have the largest positive impact on weather forecasting from any single instrument (Cardinali, 2009). However, none of the operational centers are assimilating the shortwave infrared (SWIR) radiance observations from HIR sounders, even though the SWIR radiances have more temperature sensitivity than longwave infrared (LWIR) radiances (Menzel, 2001), and were used primarily for temperature sounding retrievals in the AIRS Science Team Version 5 retrieval algorithm (Susskind et al., 2011). Nonlocal thermodynamic equilibrium (NLTE) impact on the 4.3 μm CO_2 channels can contribute more than 10 K to the observed brightness temperature (BT). Local thermodynamic equilibrium (LTE) means that the rate of energy change due to molecular collisions is larger than that due to the radiative process. This is true for all transitional and rotational energy states. However, in the upper atmosphere (i.e., above 40 km) with atmospheric density decreasing, the molecular collision rates become much less efficient to maintain the LTE for vibrational energy states, that is, the 4.3 μm CO_2 LTE band (López-Puertas & Taylor, 2001) populated by daytime solar pumping.

These sounding channels peak as high as 1 hPa (global NWP model top goes up to 0.01 hPa), providing important temperature information about upper troposphere, stratosphere, and lower mesosphere. To be able to use these SWIR radiances in data assimilation or retrieval of atmospheric soundings, the NLTE impact has to be quantified accurately.

The community radiative transfer model (CRTM), the radiative transfer for TIROS operational vertical sounder (RTTOV), and the stand-alone fast radiative transfer algorithm (SARTA) have developed fast radiative transfer models (RTMs) to simulate NLTE radiances for the 4.3 μm CO_2 band due to daytime solar pumping. Typically, this is done through a correction scheme in these models. The extra radiance coming from the NLTE effects is simulated using a fast linear regression technique, based on predictors such as solar zenith angle (SZA), local zenith angle (LZA), and some local kinetic temperatures. In this paper, the correction scheme to calculate the extra NLTE radiance component is referred to as the NLTE simulation, and the corresponding radiance component is referred to as the NLTE radiance. Similarly, the radiance simulation without NLTE effects is referred to as the LTE simulation, and corresponding radiance is referred to as the LTE radiance. The NLTE simulation is usually developed based on the NLTE model available from line-by-line RTMs (LBLRTM). So the fast NLTE simulation is limited by the representativeness of the training data sets calculated from LBLRTM. As pointed out by Matricardi et al. (2018), the NLTE effect related to excited atomic oxygen $O(^1D)$ is not included in RTTOV NLTE simulation, due to the limited representativeness of ozone mixing ratios. Limitations like that may degrade the accuracy in the fast NLTE simulation.

It is difficult to quantify the accuracy of fast NLTE simulation in RTMs due to lack of true radiance observations that are free of NLTE for validation. Common practice is to compare the background (B), defined as the calculated radiances using RTM with background (usually using NWP forecast or analysis profiles) as input, with observations (O). For example, DeSouza-Machado et al. (2007) developed a fast model to simulate NLTE. Their evaluation shows a small bias (~ −0.5 K) and standard deviation of differences (STD) (less than 1.0 K) of background minus observation (BMO) for nadir observations with SZA less than 70° globally. Yin (2016) compared calculated nominal spectral resolution (NSR) CrIS/S-NPP radiances with the CRTM using the Global Forecast System (GFS) forecast against CrIS observations over North and South Americas including the adjacent oceans. He showed that the BMO bias and STD from daytime after NLTE correction using the CRTM are comparable to those from nighttime without NLTE correction. Recently, Matricardi et al. (2018) did similar work using IASI, but with the latest version of the GRANADA NLTE population algorithm; their results showed a bias of −1.25 to 0.75 K and STD mostly less than 3.0 K when comparing the NLTE simulation using RTTOV with observations. Based on these studies, it is believed that the current fast simulation of NLTE radiance in daytime is as accurate as nighttime without NLTE.

All fast NLTE simulation studies found large discrepancies between B and O for large SZA in the high-latitude region of the winter hemisphere. DeSouza-Machado et al. (2007) and Yin (2016) attributed this large discrepancy to the decreased accuracy of NWP profiles in the upper atmosphere for high latitudes. While the discrepancy is slightly reduced, it remains quite large after replacing GFS with the European Centre for Medium-Range Weather Forecasts (ECMWF) Re-Analysis (ERA) interim data (Yin, 2016). This indicates that the NWP forecasts might not be the main source of the discrepancy. In addition, Matricardi et al. (2018) demonstrated that the profile bias is not large enough to explain the large discrepancy. Several attempts were made to establish possible reasons, but no conclusive results were reached.

In this study, a new alternative statistical method to quantify the NLTE, called Spectral Correlations to Estimate Non-Local Thermal Equilibrium (SCENTE), is introduced. SCENTE is based on observations only. It is complementary to existing fast NLTE simulations from CRTM, RTTOV, and SARTA. SCENTE can be used to improve the quantitative applications of SWIR NLTE-affected radiances in data assimilation or retrievals. The proposed work will focus on estimating NLTE radiances from full spectral resolution (FSR) CrIS observations that are affected by NLTE.

2. Limitations in NLTE CRTM Simulation

There are several limitations in existing CRTM NLTE simulations. They are lack of daytime NLTE just beyond the terminator, lack of aurora-related NLTE, possible underestimation of daytime NLTE, and possible underestimation of SWIR LTE radiances. The first two limitations should also apply to other RTM-based

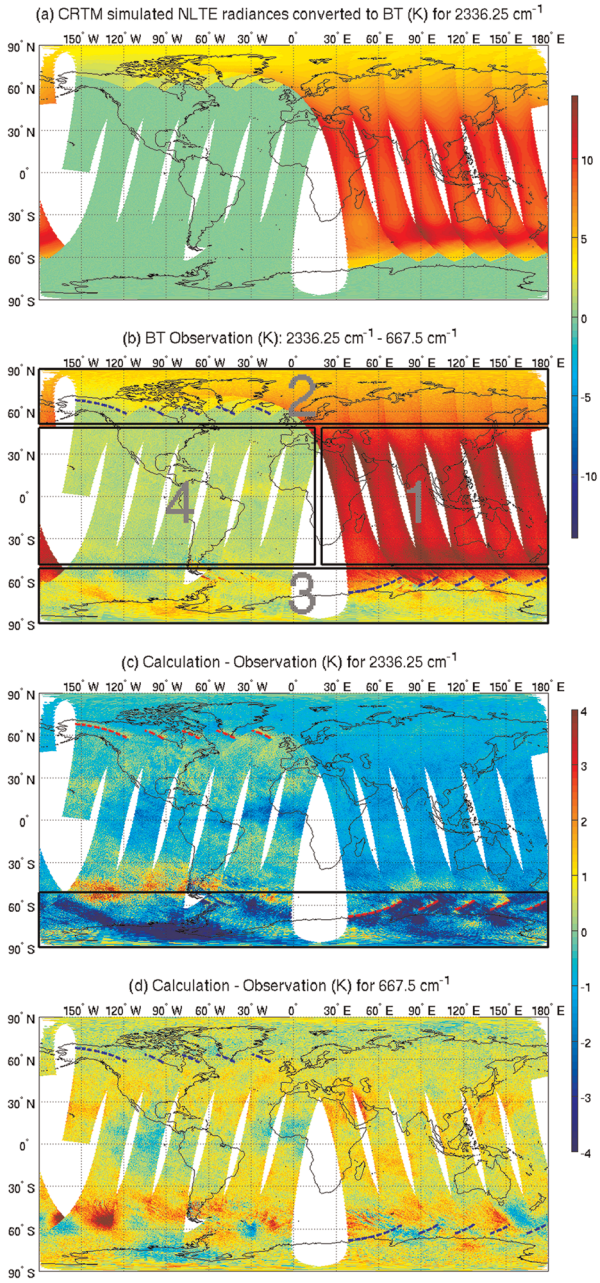

Figure 1. (a) CRTM-simulated NLTE effects in BT (K) (CRTM-simulated BT with NLTE effects turned on minus turned off), (b) the observed CrIS FSR BT differences between 2,336.25 and 667.5 cm^{-1} (former minus the latter), and the calculation minus observation of CrIS FSR BT (K) from channels of (c) 2,336.25 cm^{-1} and (d) 667.5 cm^{-1} from 00–12 UTC on 17 July 2017. The calculation is based on CRTM V 2.1.3 with ODPS coefficients, with ECMWF analysis as input, and daytime (solar zenith angle ≤90°) including NLTE effects. The blue dashed lines in (b) and (d) and red dashed lines in (c) denote the terminators. The ascending observations on right half of the imagery are mostly in daytime, and the descending observations are mostly in nighttime. Notice the large discrepancy (black rectangle in c) between observation and calculation over the South Pole region for 2,336.25 cm^{-1}, but not as large for 667.5 cm^{-1}, which is likely due to lack of aurora-related NLTE effects in the CRTM simulation. Refer to the text for details about the four regions in (b).

NLTE simulations. Figure 1a shows the simulated NLTE imagery for an SWIR channel (2,336.25 cm^{-1}) from 00 to 12 UTC on 17 July 2017 using CRTM with ECMWF analysis profiles as input. CRTM used in this study is V 2.1.3 with optical depth in pressure space (ODPS) coefficients (Chen et al., 2012). Figure 1a illustrates some known NLTE features. For example, the NLTE decreases from small SZA near the equator to large SZA near the poles, indicating that solar pumping is the main factor of the NLTE variation. Also, the NLTE appears to be stronger at the scan edge than the nadir (more evident in northern high latitudes), indicating that NLTE effects increase with LZA. That is because weighting functions peak higher with increased LZA and NLTE impact becomes stronger with altitude.

Figure 1a also shows two notable features. First, the immediate shutoff of NLTE simulations at the day/night terminator (SZA of 90°, about 62°S from 30°E to 180°E and 62°N from 160°W to 15°W) makes no physical sense, as evidenced by the discontinuity around the terminator (found in RTTOV and SARTA as well). The discontinuity is more profound around the winter terminator (in the south) than in the summer terminator (in the north). At the altitude of 50 km, where NLTE may happen, even at SZA of 95°, the atmosphere still sees the Sun, even without the consideration of solar ray bending due to atmosphere refraction. Existing RTMs assume that solar pumping is the only reason for NLTE. Therefore, there should still be NLTE beyond SZA of 90°, and one would expect a gradual decrease to zero in the simulated NLTE as the SZA increases. This limitation is mainly due to the use of LBLRTM NLTE model, which is not available for SZA beyond 90° (Chen et al., 2013).

Second, the CRTM (RTTOV and SARTA as well) assumes no nighttime NLTE. Studies (López-Puertas & Taylor, 2001; López-Puertas et al., 2004) have shown that nighttime is also subject to NLTE effects for two possible excitation mechanisms. In low-latitude to midlatitude regions, the nighttime NLTE is related to highly vibrationally excited hydroxyl radicals (OH*), although the exact excitation mechanism is still not clear (Kalogerakis et al., 2016; Sharma et al., 2015). The other mechanism for nighttime NLTE, probably the more important one causing stronger nighttime NLTE effects, is related to the high-latitude aurora activities, where the excited nitrogen N_2^* from high-energy electrons excites CO_2 (Kumer, 1977; López-Puertas & Taylor, 2001; Winick et al., 1987). Nighttime NLTE radiative transfer simulation is difficult because it relies on a complete understanding of excitation mechanisms and accurate temporal and spatial distribution of OH* and electrons. The better option might be not to use NLTE-affected SWIR radiances in assimilation or retrievals at night. So it is useful to identify SWIR radiances that are affected by nighttime NLTE effects.

Many studies have shown evidence of nighttime NLTE radiances, from rocket observations (Stair et al., 1975) and satellite limb radiometer such as Sounding of the Atmosphere using Broadband Emission Radiometry (SABER, Kalogerakis et al., 2016; López-Puertas & Taylor, 2001; López-Puertas et al., 2004; Sharma et al., 2015; Winick et al., 2004). The CrIS, as a nadir sounder, may see nighttime NLTE as well. For example, the CrIS FSR SWIR channel of 2,336.25 cm^{-1} and the LWIR channel of 667.5 cm^{-1} peak around the same altitude (50 km for U.S. standard atmosphere), and their LTE BTs are closest to each other among all CrIS SWIR/LWIR pairs. It is known that the NLTE effects on the LWIR CO_2

band are negligible. So the difference of BT (DBT) between the two channels should be a good indication of NLTE effects in the SWIR channel qualitatively.

Figure 1b shows the global imagery of DBT between the CrIS FSR SWIR channel (2,336.25 cm^{-1}) and the LWIR channel (667.5 cm^{-1}) from 00 to 12 UTC on 17 July 2017. Figure 1b can be roughly divided into four regions, illustrated by the four black rectangles. Region 1, the tropics and midlatitudes between 50°S and 50°N for ascending orbits, shows strong daytime NLTE, and the NLTE effects decrease with increased SZA, as expected for daytime NLTE effects (which is also shown in the CRTM simulation in Figure 1a). Region 2, around the summer pole, north of 50°N, mostly in daytime, shows that the NLTE effects gradually diminish with increased SZA, even beyond the terminator. CRTM depicts this gradual decrease reasonably well, but the immediate shutoff is still visible around the terminator (62°N from 160°W to 15°W). Region 3, around the winter pole, south of 50°S, mostly in nighttime, shows a totally different DBT that is much more heterogeneous than in the summer pole region. Many areas have large positive DBT, likely caused by the NLTE effects related to aurora activities (this will be better shown in section 4.1). It is important to point out that the heterogeneousness also exists on the daytime side of the terminator. The CRTM simulation in Figure 1a, on the other hand, does not show such heterogeneousness. Region 4, all nighttime between 50°S and 50°N for descending orbits, shows no large differences between the two channels, indicating that there are no strong NLTE effects in this region, consistent with the CRTM's assumption of LTE at night. These results indicate that the LTE assumption during nighttime by the CRTM causes problems, especially in the winter pole region.

The two CRTM limitations (lack of daytime NLTE just beyond the terminator and lack of aurora-related NLTE) on NLTE simulation discussed above cause significant negative biases in the simulated SWIR radiances when compared with observations, as shown in the black rectangle in Figure 1c in the high-latitude region of the winter hemisphere. The LWIR radiances, which are not affected by NLTE effects, do not see such large negative biases in the same region in Figure 1d. As will be shown in sections 5.1 and 5.2, CRTM also has two additional limitations of underestimate of SWIR LTE and NLTE radiances. In this paper, a new alternative statistical method, SCENTE, is introduced to estimate NLTE radiances directly from CrIS FSR radiance measurements, and comprehensive evaluations will be provided to analyze the various bias sources.

3. Methodology

The HIR sounders have thousands of channels, and strong correlations exist between these channels, that is, between the 4.3 μm SWIR and the 15 μm LWIR bands, both of which observe the same atmospheric CO_2. Using this correlation, one should be able to predict the shortwave radiances from the longwave radiances using a simple regression technique in the absence of NLTE, especially for nonsurface-sensitive channels. It is known that the NLTE effects on the 15 μm LWIR band are negligible (Chen et al., 2013; DeSouza-Machado et al., 2007; Matricardi et al., 2018; Yin, 2016), and hence, the SWIR radiances calculated from the LWIR will be NLTE free as well. This calculated NLTE free or LTE SWIR radiances are referred to as the predicted SWIR radiances in this study. The differences between the observed and the predicted SWIR radiances can then be used to quantify the NLTE radiances. Due to the similarity of the equation variables used in this study, the complete list is shown in Table A1 for quick reference.

3.1. The Linear Regression Technique

A simulation study using linear regression was carried out to verify that 4.3 μm SWIR LTE radiances can be predicted from the 15 μm LWIR radiances. The SeeBor database Version 5.0 (Seemann et al., 2008) with 15,704 global profiles is used to simulate the synthetic clear sky CrIS FSR radiances at 11 different LZAs: 0°, 24.62°, 33.56°, 39.72°, 44.42°, 48.19°, 51.32°, 53.97°, 56.25°, 58.24°, and 60.00°. These 11 LZAs are evenly distributed in the secant space between 0° and 60° to ensure all angles have similar weight in the training. Gaussian distributed random observation errors are added based on the sensor's in-orbit noise specification provided by Tobin et al. (2013); 90% of the database is used for training and the remaining 10% for validation.

The linear regression approach takes the form

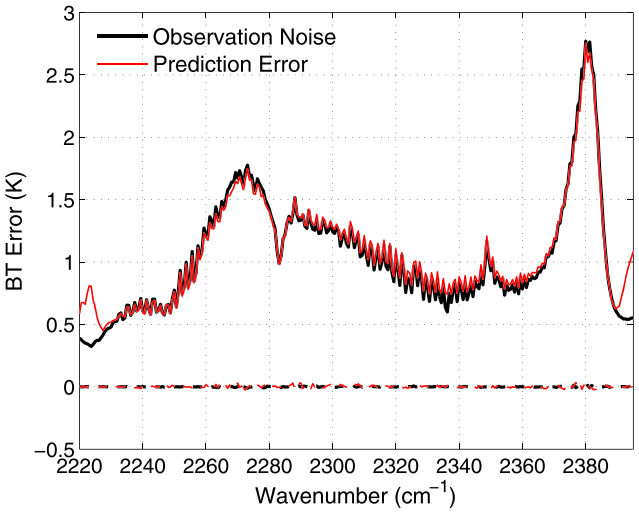

Figure 2. The validation of the prediction of SWIR LTE radiances, converted to BT (K), from LWIR ones in the absence of NLTE effects using simulated data from the SeeBor database; 90% of the data are used for training, and the remaining independent 10% are used for validation. Note that the prediction error (red solid line), the root-mean-square of differences (RMSD) of SWIR radiances between the prediction and the synthetic observation, is almost identical to the observation noise (also in RMSD, black solid line). Also shown are the mean prediction error (red dashed line) and mean observation noise (black dashed line).

$$Y = KX \tag{1}$$

where Y is the predictant, X is the predictor, and K is the regression coefficient. The predictor X is a column vector, including the first 15 eigenvalues of LWIR BT from 650–743.125 cm^{-1}, their quadratic terms (eigenvalues^2), LZA, and secant of LZA. The predictant Y is also a column vector, including the first 10 eigenvalues of SWIR BT from 2,168.125–2,418.125 cm^{-1}, and the regression coefficient K is the 2-D matrix. The static 15 eigenvectors of LWIR and 10 eigenvectors of SWIR are calculated from the training data set. Note that this correlation between SWIR and LWIR works best for sounding channels not affected by the surface. Channels affected by the surface have weaker correlations due to the complication of the surface emissivity and should not be used.

The validation results in Figure 2 show that channels between 2,230 and 2,390 cm^{-1} can be predicted quite well from the LWIR radiances. The prediction error, or the root-mean-square of difference (RMSD) of SWIR radiances between the prediction (P) and the synthetic observation, is almost identical to the observation noise (also RMSD) for those channels. Also, the prediction has zero biases.

When applying this technique to real data, several issues emerge, requiring some additional tuning of the regression (see Table 1 for the details of predictors and predictands).

1. The linear regression coefficients are derived from simulated radiances in clear sky only. So, the prediction works best for a clear sky scene. Instead of using a cloud mask to filter out cloudy pixels, all channels affected by clouds are removed. As a result, the predictor channels are limited to 60 LWIR high-altitude channels from 650–686.875 cm^{-1}, and the predictand channels are limited to 149 SWIR high-altitude channels from 2,290–2,382.5 cm^{-1}.
2. The coefficients derived from the SeeBor database do not work well in the winter pole region because of the underrepresentativeness of those extremely cold scenes from stratosphere and lower mesosphere in the training data set. It therefore requires using a training data set that better represents the real scenes. In this study, the simulated CrIS FSR radiances using CRTM with ECMWF analysis temporally and spatially interpolated to CrIS FOVs as input are used as a training data set. The accuracy of NWP individual profiles is not important. As long as the NWP profiles, as an ensemble, are a good representation of the real atmosphere, they can be used to train the linear regression. Therefore, profiles from other NWP models, analysis or forecast, can also be used. The 15 eigenvectors of LWIR and 10 eigenvectors of SWIR as well as their eigenvalues are calculated from the training data set of the simulated CrIS FSR radiances.
3. To further reduce the angle dependency, the SZA is classified into 36 equal angle intervals from −180° to 180° with negative angles representing the south side of nadir. For each SZA class, the data from nearby classes with an SZA overlap of 2.5° are included in the training to reduce the discontinuity between SZA classes. The SZA classification also helps minimize the scene-dependent bias due to the nonlinearity of the Planck function in the SWIR region. In addition, the SZA and its cosine and the latitude and its cosine are found to have positive impact on the predictions and are used as four additional predictors.

Table 1
The Predictors and Predictants of the New Linear Regression Approach to Predict SWIR Radiances From the LWIR

Predictants	10 eigenvalues of 149 SWIR channels 2,290–2,382.5 cm^{-1}
Predictors	15 eigenvalues of 60 LWIR channels 650–686.875 cm^{-1}
	Quadratic terms of the 15 eigenvalues
	Solar zenith angle
	Cosine of solar zenith angle
	Latitude
	Cosine of latitude

With the predicted SWIR eigenvalues, the predicted SWIR radiances can be calculated using

$$R_P = \varnothing_Y Y \tag{2}$$

where $\varnothing_Y$ is the static SWIR eigenvectors, calculated from the training data set, and R_P is the predicted SWIR radiances, which are NLTE free. The NLTE in observed SWIR radiances can then be estimated using

$$R_{NLTE} = R_O - R_P \tag{3}$$

where R_O is the observed SWIR radiances and R_{NLTE} is the estimated NLTE radiances. The NLTE estimation is performed for both daytime and nighttime, with the goal of better understanding the nighttime NLTE.

3.2. The Data

Two days of global CrIS FSR radiances are collected during each of the four 2017 seasons for evaluation: the spring equinox on 21–22 March, the summer solstice on 21–22 June, the fall equinox on 21–22 September, and the winter solstice on 21–22 December. The data from the four seasons are used in the statistical analysis. For each observation, two sets of CrIS FSR radiances are simulated using CRTM with ECMWF analysis as input: one with NLTE (B^C_{NLTE}, where B denotes background and the superscript C denotes CRTM) and the other with LTE (B^C_{LTE}, or without NLTE). A set of regression coefficients are generated for each season. For each season, the simulated CrIS FSR LTE radiances from the first day are used as training, and the derived regression coefficients are applied to the observations from the second day. There is no screening of the observation data except that FOVs with negative radiances are removed. The evaluation is applied globally, including different latitudes, different surface types, different LZAs, and different SZAs.

3.3. Evaluation Strategy

The evaluation compares the NLTE estimated from SCENTE with those simulated by the CRTM. Similar to previous studies, this study focuses on analyzing the BMO. For CRTM, the B comes from the LTE simulation during nighttime (SZA $>$ 90°) and from LTE plus NLTE simulations during daytime (SZA $\leq$ 90°). For SCENTE, the background B^N is calculated using (the superscript N denotes new method)

$$B^N = B^C_{LTE} + R_{NLTE} \tag{4}$$

Together with Equation 3, it can be shown that BMO for SCENTE, or δR^N, should be

$$\delta R^N = B^C_{LTE} - R_P \tag{5}$$

Meanwhile, the BMO for CRTM, or δR^C, is

$$\delta R^C = B^C_{NLTE} - R_O \tag{6}$$

It is important to point out that there are several uncertainty sources that can cause the differences between the background and observations, such as ECMWF analysis profiles, the CRTM LTE simulation (difference between true radiance observation and CRTM simulation using a true profile), the estimated or simulated NLTE radiances, and the radiance observations. The following section shows the statistical comparison of BMO from the CRTM and SCENTE. Detailed discussion about the various sources of biases is presented as well.

4. Evaluation

4.1. Case Demonstration

SCENTE is applied to the real data from 00 to 12 UTC on 17 July 2017 shown in Figure 1. Figure 3a shows the NLTE radiances estimated from SCENTE. Overall, the geographic pattern matches better with Figure 1b than the CRTM simulation in Figure 1a. The new estimated NLTE radiances are large during the daytime between 50°S and 50°N. They gradually approach zero in the summer pole region and are highly heterogeneous in the winter pole region. In the winter pole region, there appears to be additional NLTE contributions other than those related to solar pumping, likely due to aurora activities. Most of the nighttime radiances between 50°S and 50°N show no obvious NLTE effects. The better agreement with Figure 1b is indicative of the promising potential of SCENTE.

To further evaluate the estimated NLTE radiances from SCENTE, Figure 3b shows the BMO. Figure 3b shows that calculations agree well with observations for almost the whole globe, with absolute differences mostly less than 1 K, in both daytime and nighttime, except the winter pole region, south of 40°S. However, comparing Figure 3b with Figure 1c, the differences in the winter pole region from SCENTE are much

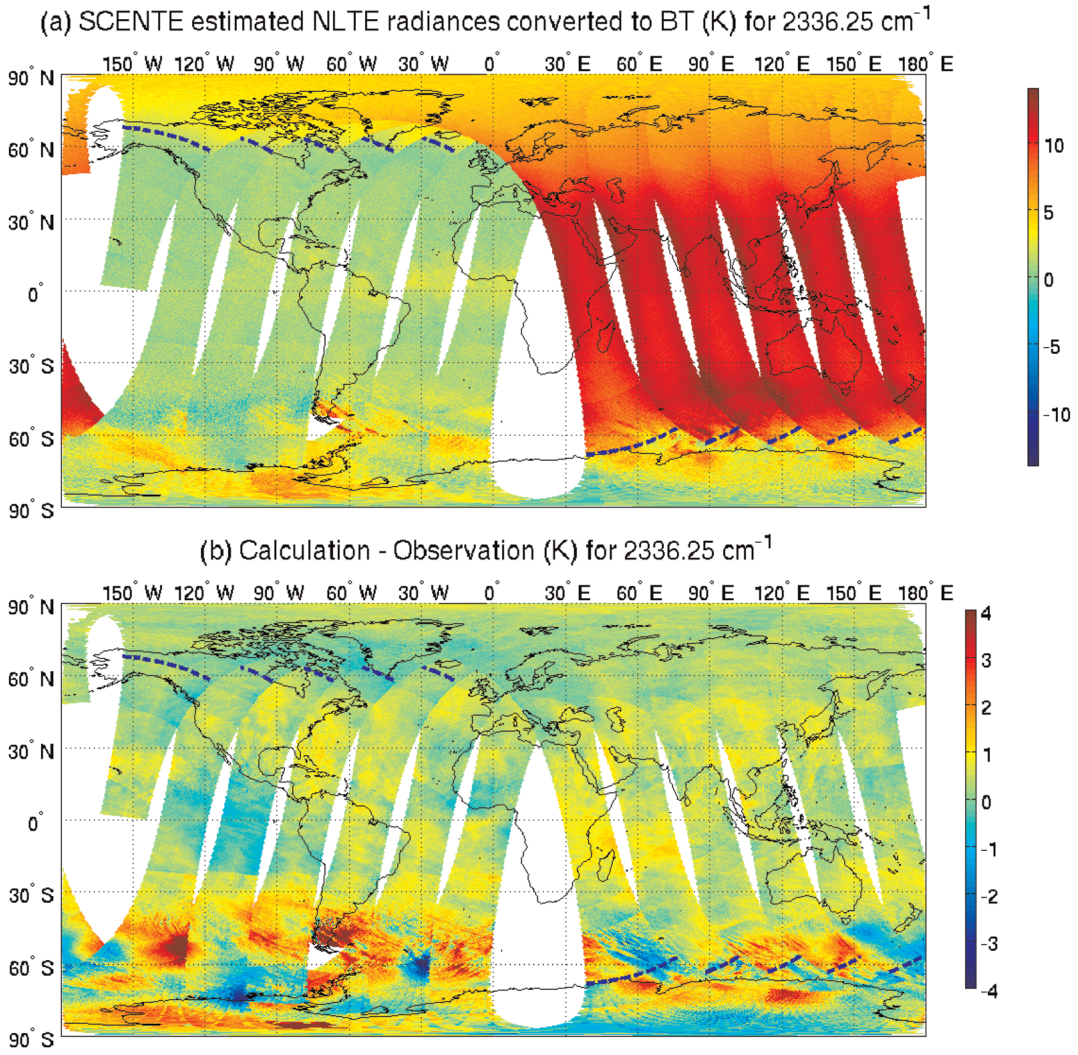

Figure 3. (a) The estimated NLTE radiances converted to BT (K) and (b) BMO of CrIS FSR channel of 2,336.25 cm^{-1} from SCENTE from 00 to 12 UTC on 17 July 2017. Note that the color bars are different in the two panels. The blue dashed lines denote the terminators.

smaller in magnitude than those from the CRTM simulation. And SCENTE shows both negative and positive differences, while the CRTM simulation shows mostly large negative differences (dark blue). As pointed out earlier, the winter pole region may be subject to aurora-related NLTE, which is mostly during the night. Without aurora-related NLTE in the CRTM simulation, results significantly underestimate the SWIR radiances, while SCENTE shows substantially better agreement. In addition, unlike the CRTM simulation, SCENTE shows no discontinuity of BMO near the terminator in the South Pole region.

While these qualitative evaluations favor SCENTE, there is no supporting evidence that the NLTE effects in the winter pole region are actually related to aurora activities, especially in nighttime. It is known that the Visible Infrared Imaging Radiometer Suite (VIIRS) day/night band (DNB) is capable of detecting extremely low amounts of visible lights at night, such as auroras (Seaman & Miller, 2013). Figures 4a and 4c show the logarithm of VIIRS DNB radiances from S-NPP. For these two particular passes, the strong aurora activities are clearly seen as the red stripes off the Antarctic coast. Note that the deep red area is daytime. The estimated NLTE radiances using SCENTE, in Figures 4b and 4d, match well with the strong aurora activities geographically. These results indicate that the aurora-related nighttime NLTE effects are fairly significant, with magnitudes up to 6 K in BT. While Figure 4 shows a good example of nighttime strong aurora

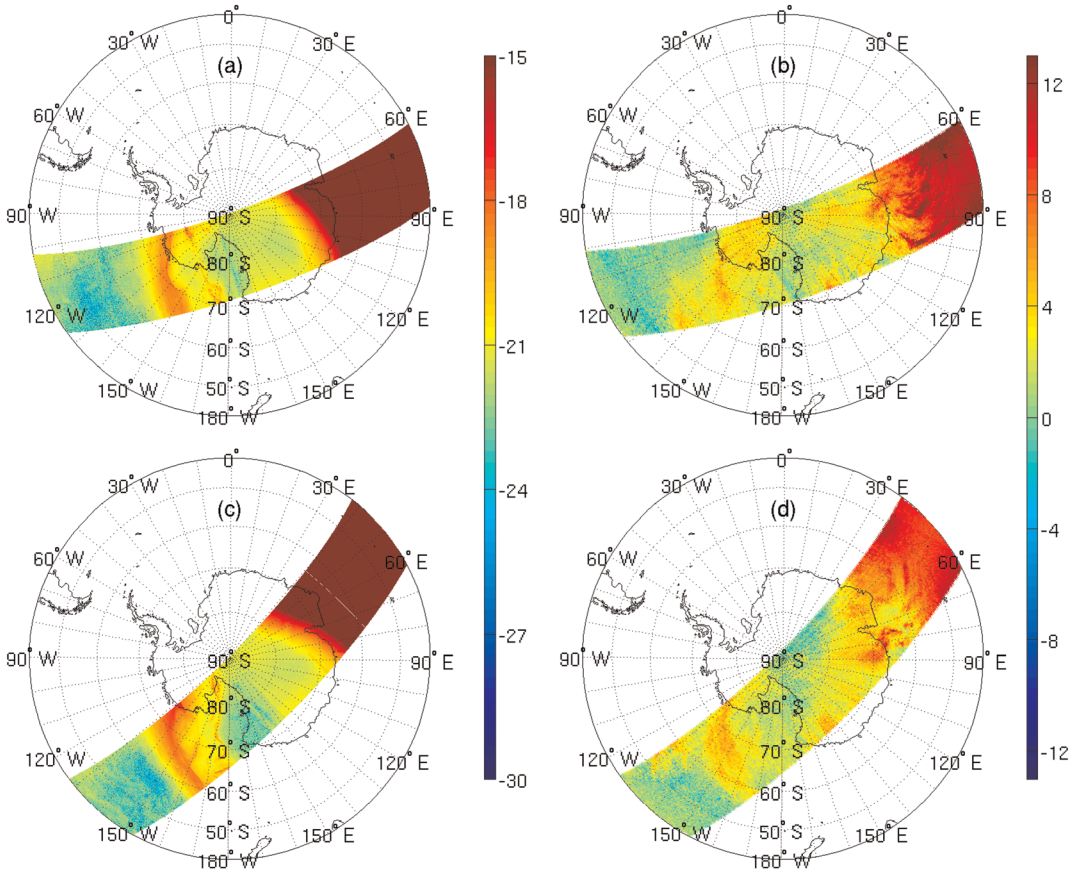

Figure 4. (a, c) The logarithm of VIIRS/S-NPP day/night band radiances (W/cm^2/sr) and (b, d) the estimated NLTE radiances (converted to BT in K) of CrIS FSR channel 2,336.25 cm^{-1} using SCENTE on 17 July 2017. Two passes are shown: upper for 0840 UTC and bottom for 1023 UTC. Note that the deep red areas in (a) and (c) are daytime in ascending orbits.

activities, aurora is not limited to nighttime. Daytime strong aurora should have similar impact on NLTE radiances. The absence of daytime aurora-related NLTE could be one potential reason causing the large discrepancy between simulation and observation for large SZA reported by several studies (DeSouza-Machado et al., 2007; Matricardi et al., 2018; Yin, 2016). Without proper handling of the aurora-related NLTE effects, the affected CrIS SWIR radiances cannot be used quantitatively in assimilation or retrievals. Although not shown, the Arctic region near winter solstice sees similar matching between nighttime NLTE and aurora activities.

4.2. Statistical Analysis

As mentioned before, for each season, 1 day of data is used as training, and the derived coefficients are applied to the other day. Figure 5 shows the statistics of bias and STD of BMO during the day. For all of the four seasons, the STDs from SCENTE and CRTM are comparable, and both are slightly larger than the noise equivalent delta temperature (NEdT). The spectral variations of the STD also follow similar patterns as NEdT, indicating that both methods depict the daytime NLTE well, especially spectrally. However, comparison of the biases reveals much larger differences between the two methods. For all of the four seasons, the spectral mean biases are equal or smaller than 0.21 K in absolute values from SCENTE, for all SWIR channels. And they show only weak spectral variations. The CRTM, on the other hand, shows significant negative biases as well as substantial spectral variations. The CRTM spectral mean bias is as large as −1.48 K. As will be shown in sections 5.1 and 5.2, the main sources for these biases are CRTM LTE simulation and CRTM NLTE simulation.

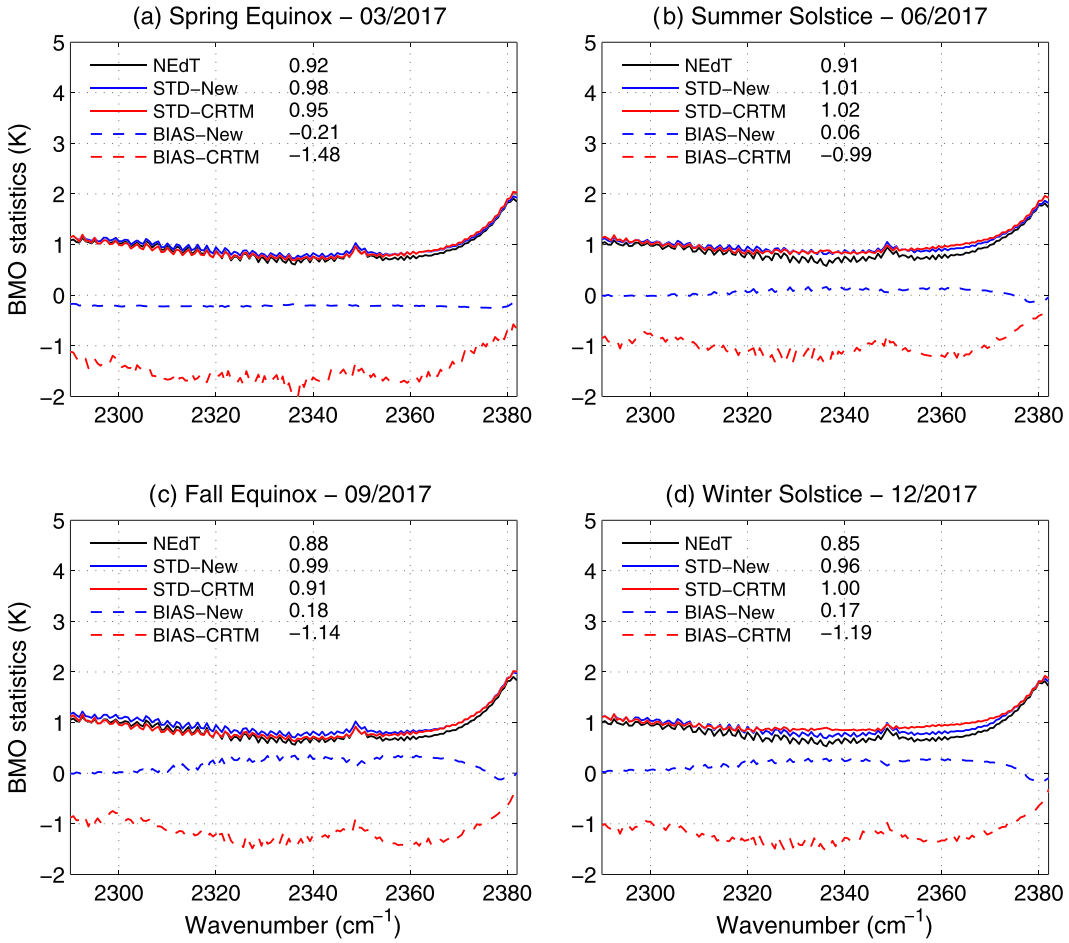

Figure 5. The bias (dashed lines) and standard deviation (solid lines) of BMO from CRTM simulation (red) and SCENTE (blue) for daytime (solar zenith angle ≤90°) of four typical season days: (a) spring equinox, (b) summer solstice, (c) fall equinox, and (d) winter solstice, along with NEdT (black solid line). The numbers to the right of the legends are the spectral average in kelvin.

Figure 6 shows the corresponding statistical results for nighttime. For all of the four seasons, the STDs from SCENTE are still slightly larger than NEdT and significantly smaller than the CRTM. Especially for the summer solstice case, the spectral mean CRTM STD is 0.69 K larger than SCENTE and 0.81 K than NEdT. It appears that the STD differences between the CRTM and SCENTE are much larger for the two solstice cases than the two equinoxes. That is likely due to possible nighttime NLTE in extremely cold scenes in the winter pole as shown in Figure 1b. The biases again are close to zero from SCENTE for all four seasons, with the maximum absolute spectral mean of 0.23 K in the spring equinox. For the CRTM simulation, the biases are somehow smaller for spring and fall, but summer and winter still are around −1.0 K.

Comparing the spectral mean bias in Figures 5 and 6 reveals that the biases from SCENTE show little diurnal variations. The summer solstice appears to have the largest diurnal variation of 0.13 K in spectral mean bias, with less than 0.03 K for all other three seasons. However, the CRTM simulation shows significant diurnal variations. For spring equinox, the spectral mean bias is reduced by 0.84 K from day to night, and for fall equinox, it is reduced by 0.6 K. Summer solstice sees smallest diurnal variation of 0.20 K in spectral mean bias among the four seasons, still much larger than the largest diurnal variation season from SCENTE. These strong diurnal variations of BMO biases can pose problems for radiance assimilation in NWP applications as current bias correction scheme does not explicitly handle such variations. The daytime biases have two main sources: the CRTM LTE simulation and the CRTM NLTE simulation, both of which have

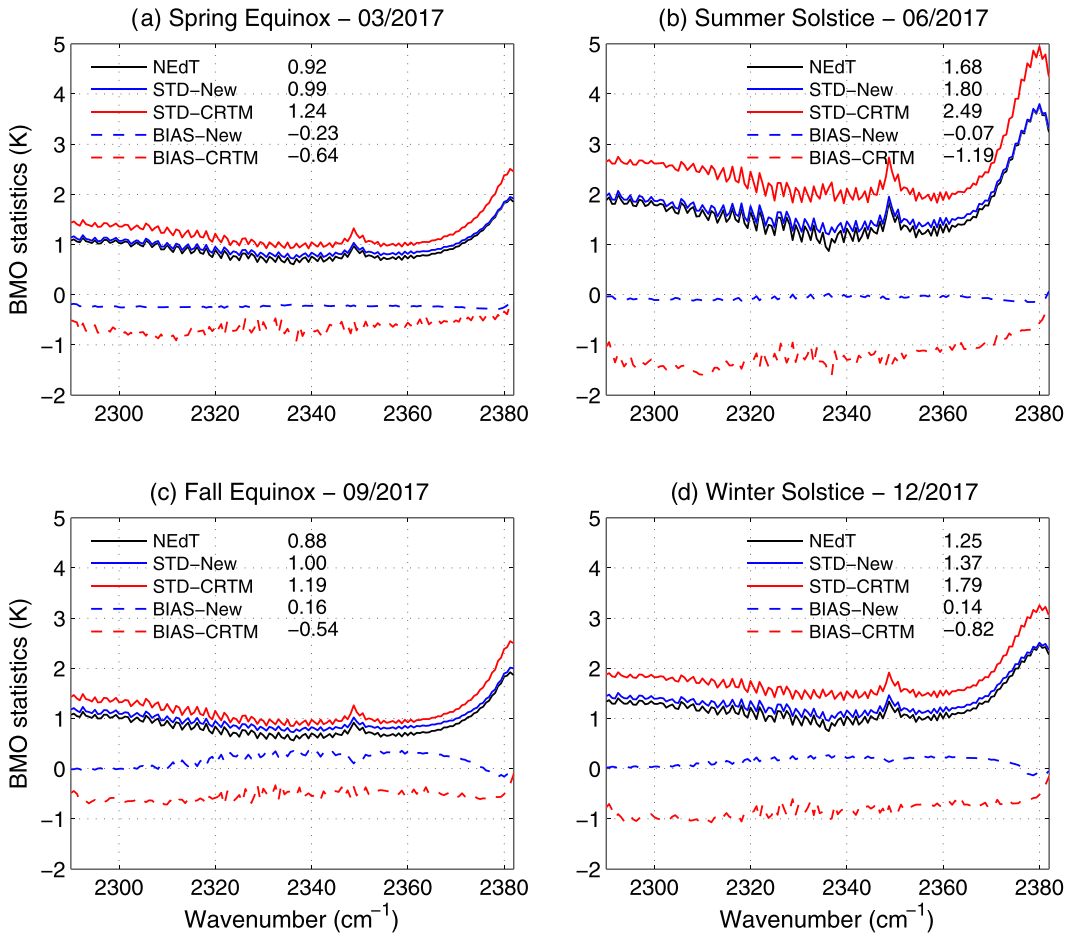

Figure 6. Similar as Figure 5 but for nighttime.

about 0.5 to 1.0 K negative biases (as will be shown in sections 5.1 and 5.2). The nighttime biases also have two main sources: the CRTM LTE simulation and the absence of NLTE consideration (negative bias as well). The fact that the two equinoxes have less negative biases than the two solstices might indicate that the nighttime NLTE is more significant for solstices than equinoxes. Both Figures 5 and 6 show increased NEdT and STDs around 2,380 cm^{-1}. That is because those channels are sounding tropopause, having colder BTs than others.

These results suggest that SCENTE is superior to the CRTM simulation, with smaller biases during daytime and nighttime, smaller STDs during nighttime, and weaker diurnal variation of biases. However, as will be shown in section 5, there are substantial biases in the estimated NLTE from SCENTE.

5. Discussion

The biases shown in Figures 5 and 6 can come from four possible sources: the observation, the CRTM LTE simulation, the CRTM NLTE simulation, and the ECMWF analysis profiles. In this study, the CRTM LTE bias refers to the CRTM bias from the CRTM LTE simulation assuming that there is no bias in the input profiles, and CRTM NLTE bias refers to the bias from the CRTM NLTE simulation assuming that there is no CRTM LTE bias and no profile bias. Calibration studies have proven the good accuracy of the CrIS radiance observations. Its main source of bias is lack of polarization correction (Taylor et al., 2018). The CrIS FSR radiance data used in this study have not been polarization corrected; comparisons have been carried out to examine the impact of this. The results show that the uncorrected radiance observations have small

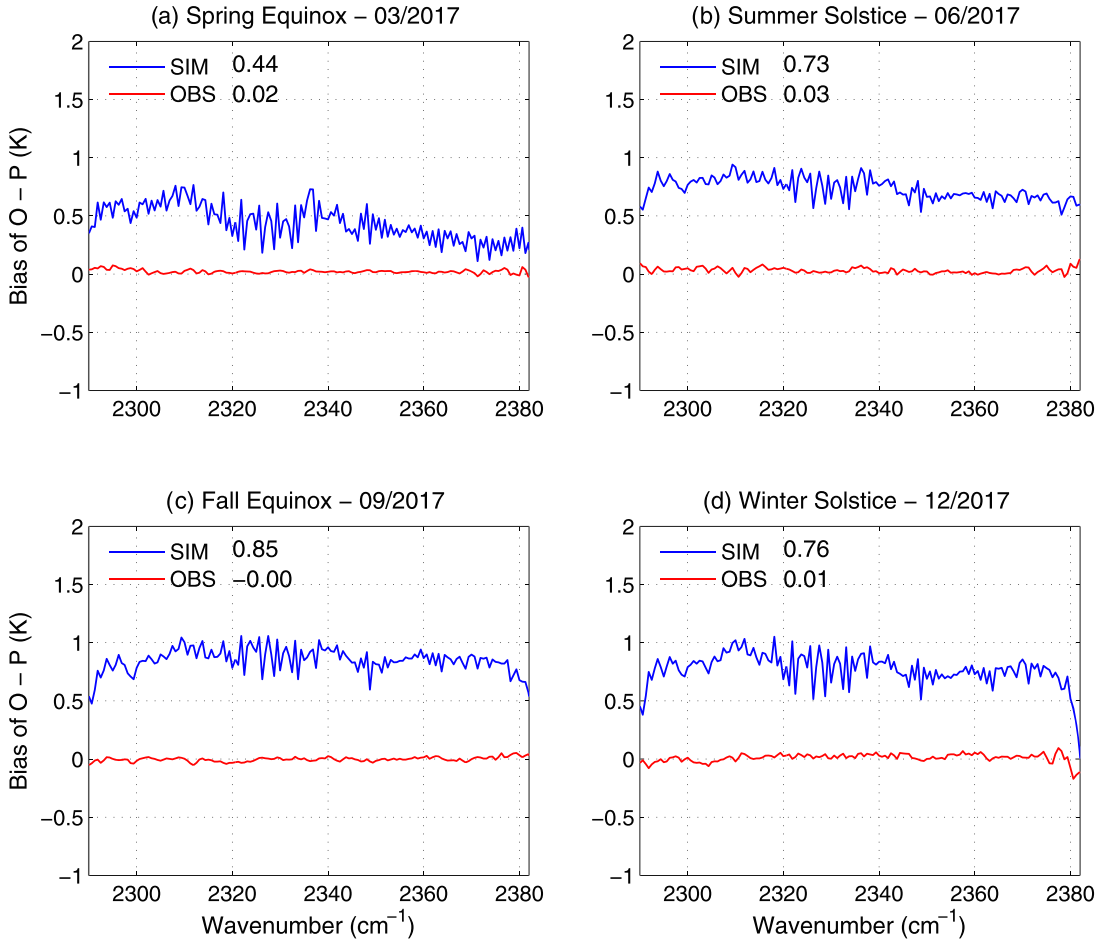

Figure 7. The bias in the estimated NLTE radiances (converted to BT in K) in CrIS FSR SWIR radiances using SCENTE, with coefficients derived from simulated (blue) or observed (red) radiances in the training, for deep night (solar zenith angle ≥150°) of the four typical season days: (a) spring equinox, (b) summer solstice, (c) fall equinox, and (d) winter solstice. The numbers to the right of the legends are the spectral average in kelvin.

positive biases, mostly less than 0.2 K in BT, with slightly more at nighttime than daytime. These biases are much smaller than those shown in Figures 5 and 6; their impact on the bias analysis is small and thus not discussed further in this study.

5.1. NLTE Bias From SCENTE

Figure 3a shows that the differences between observation and prediction for deep night (SZA ≥ 150°) are close to zero, indicating that the deep night NLTE for those regions is likely negligible. One method to verify this is to use observed radiances instead of simulated radiances in the training. For each of the 2 days of the four seasons, observed LWIR and SWIR radiances from deep night of the first day are used as training. And the derived regression coefficients are applied to the deep night of the second day for independent evaluation. For different seasons, the latitude range of the deep night is different. But the approximate range is between 30°S and 30°N. Figure 7 shows the biases of observation-minus-prediction (OMP) or the estimated NLTE radiances using SCENTE with regression coefficients derived from observed radiances as well as simulated radiances. For all of the four seasons, when observed radiances are used in the training, the biases of OMP are almost zero, which is unlikely to happen if deep night NLTE is not negligible. Figure 7 also shows that substantial positive biases (about 0.70 K in four season mean) are presented in OMP, when simulated radiances are used for training. This indicates that substantial negative biases exist in the predicted SWIR radiances compared with observation. The same biases should be present in the predicted SWIR radiances

for daytime, causing overestimates of the NLTE radiances by 0.70 K. However, this is only true for the area where the LWIR radiances are similar to the deep night, that is, tropics and nearby midlatitudes between 30°S and 30°N. Beyond that, it is not clear how large the estimated NLTE biases are.

As a linear regression technique, SCENTE itself does not introduce biases, as shown in Figure 2. However, if there are biases in the training data sets from CRTM LTE simulation, those would be transferred to the predicted SWIR LTE radiances, and thereafter causing biases in the estimated NLTE radiances, when applied to real data. The predicted SWIR radiances have two CRTM LTE bias sources: the predictands of SWIR radiances and the predictors of LWIR radiances. Comparing CRTM LTE simulation with observations for deep night (NLTE free) shows that the CRTM LTE bias in SWIR is much larger than that in LWIR in absolute value. Studies by Ding et al. (2011) and Liu et al. (2019) also show that CRTM LWIR simulation is accurate. Thus, the predicted SWIR LTE radiances, R_P, are most likely subject to the CRTM LTE bias in SWIR. The CRTM-simulated LTE radiances B^C_{LTE}, on the other hand, are subject to CRTM LTE biases in SWIR and ECMWF analysis biases. The difference between B^C_{LTE} and R_P, therefore, should be mostly subject to ECMWF analysis biases. Figures 5 and 6 show that the biases of the BMO for the estimated NLTE radiances from SCENTE, or δR^N, or $B^C_{LTE} - R_P$, are close to zero for both daytime and nighttime. This is also true for the tropics and nearby midlatitudes between 30°S and 30°N (not shown). These results indicate that (1) the CRTM LTE bias in SWIR is the main bias source causing bias in the predicted SWIR radiances and (2) the ECMWF analysis bias is small and negligible. The above discussions indicate that SCENTE overestimates the NLTE radiances by 0.70 K in BT in the tropics and nearby midlatitudes. And those positive biases are introduced in the training, where the CRTM underestimates LTE radiances by 0.70 K in BT.

It is not immediately clear what causes CRTM to underestimate the CrIS SWIR LTE BT by 0.7 K. One possible reason is that the CRTM CO_2 default value used in this study is smaller than the CO_2 concentration in 2017. Those CrIS SWIR channels are mostly sensitive to stratospheric CO_2, which is slightly smaller than that in the troposphere. According to Diallo et al. (2017), the CO_2 concentration in the stratosphere increases at a slightly smaller trend (about 1.85 ppmv/yr for stratosphere from 16 to 43 km from 2000 to 2010) than in the troposphere (about 2.0 ppmv/yr). The tropospheric CO_2 concentration is about 405 ppmv in 2017, while the CRTM default value is about 384 ppmv. So the stratospheric CO_2 concentration is underestimated by about 20 ppmv due to the use of the CRTM default value. Because the atmospheric temperature increases with altitude in the stratosphere, the underestimation of stratospheric CO_2 concentration leads to an underestimate in the simulated CrIS SWIR LTE BT. To quantify that, a sensitivity study is carried out using CRTM with the SeeBor database. The results show that the spectral average of BT increase is about 0.1 K for both SWIR and LWIR when the CO_2 concentration profile is increased by 10 ppmv. Since the CO_2 concentration is underestimated by about 20 ppmv in the CRTM simulation, that means the underestimation of CRTM LTE BT by 0.7 K found in this study could be partially explained (in about 0.2 K) by the use of the CRTM default CO_2 concentration.

It is worth noting that the CRTM default CO_2 concentration is also used in generating the training data set in this study. However, that has little impact on the SCENTE prediction, meaning there is no obvious bias introduced in the SCENTE-predicted SWIR LTE radiances or the SCENTE-estimated NLTE radiances due to the use of the CRTM default CO_2 concentration in the training data set. To confirm that, a sensitivity study is carried out. A new set of synthetic CrIS FSR LTE BT observations are simulated using CRTM with CO_2 concentration of 400 ppmv (the max allowed by CRTM) from the SeeBor database. The coefficients from Figure 2 (default CO_2 concentration used) were applied to the new synthetic CrIS BT observations. The results show that the SWIR LTE radiances can be accurately predicted from LWIR radiances with no obvious bias introduced (not shown). That indicates that the use of the CRTM default CO_2 concentration does not cause an additional bias in the SCENTE prediction.

5.2. CRTM NLTE Biases

This section focuses on quantifying the CRTM NLTE biases using a double difference technique (Li et al., 2010, 2012). While BMO has been used to evaluate the performance of RTM-simulated NLTE radiances (Chen et al., 2013; DeSouza-Machado et al., 2007; Matricardi et al., 2018), no studies have quantified the biases in RTM-simulated NLTE radiances. The difficulty is due to the fact that the biases in BMO have three major sources: CRTM LTE biases, CRTM NLTE biases, and atmospheric profile biases, none of which are

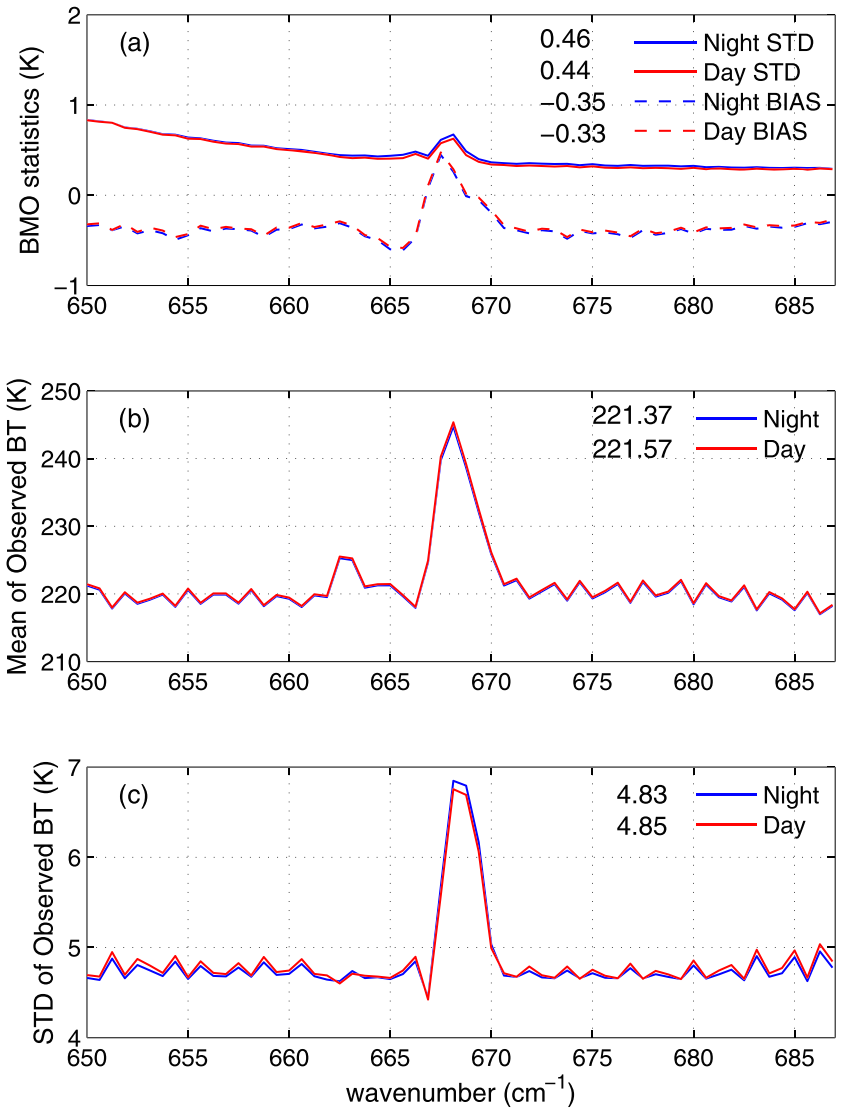

Figure 8. (a) The bias (dashed, K) and standard deviation (solid, K) of BMO, (b) the mean observed radiances, converted to BT (K), and (c) the standard deviation of observed radiances (K), converted to BT (K), for daytime and nighttime of CrIS FSR channel of 667.5 cm^{-1} for all of the four typical season days together between 60°S and 60°N. The numbers to the left of the legends are the spectral average in kelvin.

known accurately. A double difference technique, more specifically, the day/night difference of BMO, offers an opportunity to minimize the impact from CRTM LTE biases and the input atmospheric profile biases and maintain the CRTM NLTE biases.

To demonstrate this, all four seasons of data with latitudes between 60°S and 60°N are used. This region is selected because there is little day/night difference in CRTM LTE biases and the input atmospheric profile biases, as will be demonstrated. Figure 8a shows that there is little day/night difference in LWIR BMO biases (STD as well), and Figure 8b shows that there is little day/night difference in LWIR *O* mean values (STD as well). These results indicate that there is little day/night difference in the LWIR *B* biases. The LWIR *B* has two major bias sources: the CRTM LTE biases and the ECMWF analysis profile biases. CRTM LTE bias is caused by the CRTM LTE simulation, assuming that there is no bias in the input profiles. It should not change much if the profiles do not change dramatically. Figure 8b shows that there is little day/night difference in the mean LWIR observed radiances, indicating that the true upper atmospheric profiles do not change much from

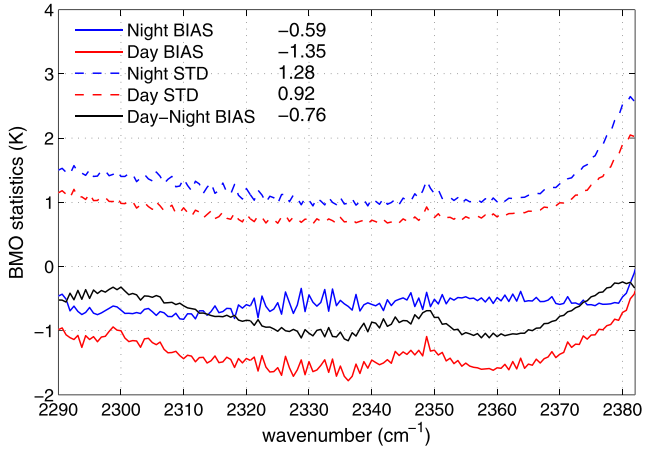

Figure 9. The bias (solid, K) and standard deviation (dashed, K) of BMO for daytime (red) and nighttime (blue) of CrIS FSR channel of 2,336.2.5 cm^{-1} for all of the four typical season days together between 60°S and 60°N. The night/day difference of the bias (night-day, in black) denotes the CRTM NLTE bias for the region. The numbers to the right of the legends are the spectral average in kelvin.

daytime to nighttime. It does not matter if ECMWF analysis profiles are highly accurate or not. As long as they are reasonably accurate, the CRTM LTE bias should not change much from daytime to nighttime. In other words, the ECMWF profiles may have some bias during the day, and some other bias at night, their impact on the CRTM LTE bias is small. Therefore, it is reasonable to believe that there is little day/night difference in the CRTM LTE bias. Since there is little day/night difference in LWIR BMO biases, then there is little day/night difference in ECMWF analysis profile biases as well. These results explain why there is little day/night difference in the CRTM LTE bias in LWIR. For SWIR, it is reasonable to expect little day/night difference in CRTM LTE biases as well.

Figure 9 shows the biases and STDs of the SWIR BMO of both daytime and nighttime for the four season days together. Daytime has smaller STDs because of smaller observation noise in the BT domain. Note that they are nearly identical in the radiance domain because CrIS noise equivalent delta radiance has no scene dependency (Zavyalov et al., 2013). The spectral mean of daytime biases is −1.35 K, significantly greater than the nighttime spectral mean of −0.59 K. For SWIR, the biases of BMO have three major sources: the CRTM LTE bias, the CRTM NLTE bias, and the ECMWF analysis profile bias. As discussed before, there is little day/night difference in the CRTM LTE biases and the ECMWF analysis profile biases. The day/night difference in the SWIR BMO biases should be mostly caused by the difference in CRTM NLTE biases. While Figures 1 and 3 show that there are possible nighttime NLTE radiances around 50°S, examination of individual season reveals that the majority of the region between 60°N and 60°S is free of strong nighttime NLTE. The assumption of no NLTE for nighttime between 60°N and 60°S should not introduce much of a bias in SWIR *B* calculation. Therefore, the day/night difference of the BMO biases should be dominated by the daytime CRTM NLTE bias, which underestimates the NLTE by 0.76 K. It is important to point out that the estimated CRTM NLTE bias is the mean bias for the four typical season days and latitudes between 60°N and 60°S. The CRTM NLTE bias outside this region could be substantially different.

5.3. The Static Coefficients

Ideally, the regression coefficients need to be updated regularly to ensure optimal results by using a training data set that is as relevant as possible, as shown in Figures 5–9, where an individual set of regression coefficients are derived and applied for each season, referred as dynamic regression coefficients. However, a set of static regression coefficients are desired for NWP data assimilation applications because frequent coefficient updates would represent a "shock" to the system, which should be avoided. The static regression coefficients can be obtained by using all four seasons of training data sets together. The predicted SWIR LTE radiances are compared for static and dynamic regression coefficients in Figure 10, with the classification of SZA. For all SZAs, the mean differences are very small, less than 0.1 K in absolute value for almost all channels, or less than 0.03 K in absolute value for spectral mean. Figure 10b shows that different SZAs have different STDs. The SZAs of 0–30° (0.16 K of spectral mean) and 30–60° (0.21 K of spectral mean) have the smallest STDs, the SZAs of 60–90°, 90–120°, and 120–150° have the largest STDs (0.37 to 0.41 K of spectral mean), and the deep night SZAs of 150–180° are in the middle (0.28 K of spectral mean). The larger STDs are associated with colder scene temperatures, indicating that observation noise is an important factor contributing to STDs.

Those substantial STDs (0.1 to 0.5 K) in Figure 10b do not necessarily mean reduced accuracy in the predicted SWIR LTE radiances by using the static regression coefficients. Figure 11 shows the statistics of biases and STDs of BMO using the static and dynamic regression coefficients. For all four seasons of data together, using static regression coefficients does not appear to increase the biases and STDs, for both daytime and nighttime, although slightly increased biases and STDs are visible around 2,380 cm^{-1}. The spectral means are also almost identical. Examination of individual classes of SZA (not shown) reveals that colder scenes see slightly increased STDs (less than 0.05 K), indicating that the static regression coefficients are slightly more sensitive to the observation noise, which may slightly reduce the accuracy of the predicted SWIR

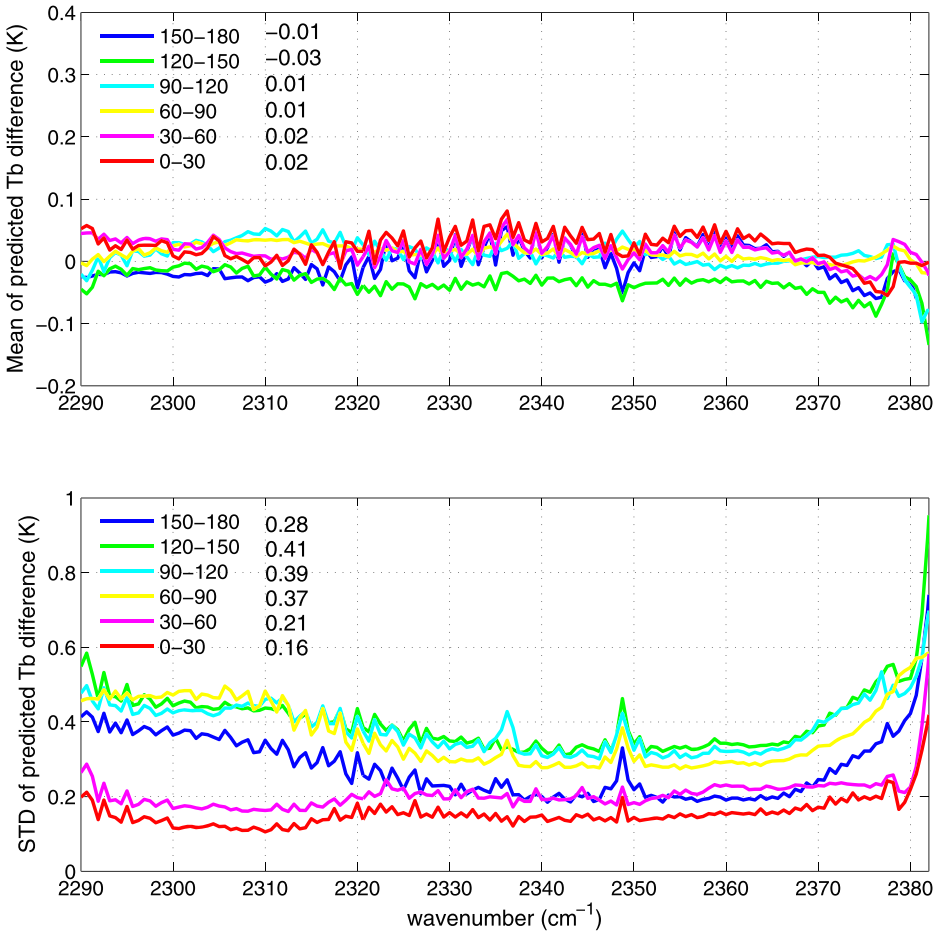

Figure 10. (a) The mean (K) and (b) the standard deviation (K) of the differences of the predicted SWIR LTE radiances, converted to BT (K), between the static and the dynamic regression coefficients with the classification of solar zenith angle (°) for all the four typical season days in 2017. The numbers to the right of the legends are the spectral average in kelvin.

LTE radiances. However, as shown in Figure 11, the accuracy reduction is very small. Therefore, the static regression coefficients can be used instead of the dynamic ones.

5.4. Limitations and Potential Applications

The ultimate goal of accurately estimating SWIR NLTE radiances is to provide accurate SWIR LTE radiances that can be directly used in data assimilation or retrievals. While SCENTE presented in this study provides an alternative method for estimating NLTE radiances with good accuracy, application could be somewhat limited. One limitation is that SCENTE directly estimates the SWIR LTE radiances from the LWIR radiances. Thus, information content is no larger than what is already contained in the LWIR radiances. Therefore, caution should be used for quantitative application of the SCENTE-estimated SWIR LTE radiances. Second, SCENTE may introduce an additional potential source of representativeness error to the SWIR radiances due to the use of LWIR radiances as predictors, which is not desirable in data assimilation. The third limitation is that the estimated NLTE radiances may contain more information than NLTE. As a matter of fact, the estimated NLTE radiances contain all information that cannot be predicted from the LWIR radiances, including SWIR NLTE impact and trace gas impact (i.e., CO and N_2O for SWIR

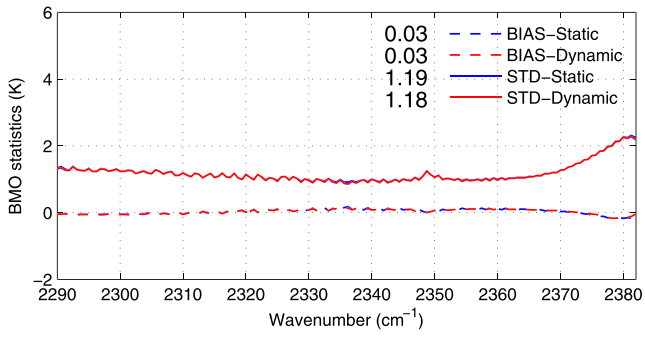

Figure 11. The bias (dashed lines) and standard deviation (solid lines) of BMO from SCENTE using static (blue) and dynamic (red) coefficients for both daytime and nighttime of four typical season days: spring equinox, summer solstice, fall equinox, and winter solstice of 2017. The numbers to the left of the legends are the spectral average in kelvin.

and O_3 for LWIR). Finally, this study is limited to 149 SWIR channels that peak high in stratosphere and lower mesosphere to reduce the cloud contamination. Although this has covered most of the NLTE-affected channels, future work will expand to more SWIR channels that are affected by NLTE and clouds. However, these limitations do not render that SCENTE is not useful.

Quantitative applications of SWIR NLTE-affected radiances rely on accurate RTM simulations. This study shows that the RTM-based SWIR NLTE radiance simulation is reasonably accurate for most of the daytime and also has negligible NLTE impact for most of the nighttime. However, there are some limitations, such as increased discrepancy over high latitude in winter polar region, the unrealistic cutoff of NLTE simulation at the terminator of the SZA of 90°, and the lack of aurora-related NLTE. SCENTE, providing an alternative way to estimate NLTE radiances, can be used together with the RTM-based NLTE radiance simulations to improve the quantitative applications of the SWIR NLTE-affected radiances. For example, NLTE radiances estimated by SCENTE may be used to bias correct the RTM-based NLTE radiances because SCENTE shows low BMO biases. Also, SCENTE can be used to quality control the RTM-simulated NLTE radiances to determine which simulation is accurate enough for data assimilation or retrievals. This quality control may be applied both daytime and nighttime, as this study shows that possible nighttime NLTE is not negligible, especially over winter polar regions.

6. Summary

Accurate fast NLTE RTM simulations are needed in order to quantitatively use SWIR radiance observations. Despite overall good agreement between calculations or background (B) and observations (O), four potential limitations are demonstrated using CRTM as an example: (a) lack of daytime NLTE just beyond terminator, (b) lack of aurora-related NLTE, (c) possible underestimation of SWIR NLTE radiances in daytime, and (d) possible underestimation of SWIR LTE radiances. It is important to point out that the underestimates of NLTE and LTE radiances are referred to CRTM only. Other RTMs may have different bias behaviors. Understanding LTE and NLTE biases in RTMs is important for SWIR radiance assimilation because NWP models prefer stable diurnal bias. In this paper, a new method, called SCENTE, is presented to estimate NLTE radiances, based on prediction of SWIR radiances from LWIR radiances in the absence of NLTE effects. The differences between the observed and the predicted SWIR LTE radiances are then used to characterize the NLTE radiances.

SCENTE is demonstrated with four seasons (2 days from each season) of global CrIS FSR radiance observations. The statistical analysis of BMO shows that SCENTE has comparable STDs as the CRTM simulation for daytime; both are very close to observation noise indicating reasonable characterization of the NLTE radiance spectrum. For nighttime, SCENTE shows STDs comparable to observation noise, but CRTM simulation shows substantially larger STDs. The larger nighttime CRTM simulation STDs are likely caused by two limitations: (a) the scenes beyond the terminator of SZA of 90° where the stratosphere and mesosphere still see the Sun and are subject to possible solar NLTE effects, while CRTM assumes no NLTE, and (b) the lack of aurora-related NLTE, which may exist in both daytime and nighttime.

Detailed investigation is carried out to analyze the biases in SCENTE-estimated NLTE radiances. It is found that SCENTE overestimates the daytime SWIR NLTE radiances by 0.70 K in BT for latitudes between 30°S and 30°N. These positive biases are due to the training data sets from CRTM LTE simulations, which underestimate LTE radiances by 0.70 K in BT. Up to 0.2 K out of 0.7 K is due to the underestimation of CO_2 concentration by the CRTM default value. However, when comparing B with O, or LTE B and the predictions for SWIR, because they are both subject to the same LTE biases, the BMO shows very small biases (mostly less than 0.3 K in absolute values). A double difference technique is used to estimate the biases in the CRTM-simulated NLTE, and the results show that CRTM underestimates NLTE by 0.76 K for latitudes between 60°S and 60°N.

Application of SCENTE is somewhat limited because the predicted SWIR radiances represent information already contained in the LWIR radiances. Caution should be used for any quantitative application. However, SCENTE provides an alternative way to estimate SWIR NLTE radiances, independent of and complementary to the RTM-based simulation. It can be used together with existing methods to improve the quantitative application of SWIR radiance observations, that is, quality control and bias correction of the RTM-based NLTE simulation, for data assimilation or retrievals.

Appendix A

Table A1
The List of the Variables Used in the Equations

R_{NLTE}	NLTE brightness temperature in (K) from SCENTE. This is NLTE component only and does not include LTE contribution
B^C_{LTE}	The CRTM-calculated shortwave infrared LTE brightness temperature (K)
B^C_{NLTE}	The CRTM-calculated shortwave infrared brightness temperature (K), including both LTE and NLTE
B^N	The calculated shortwave infrared brightness temperature (K) from SCENTE, including LTE and NLTE
K	Regression coefficients in 2-D matrix
R_P	Predicted shortwave infrared brightness temperature (K)
R_O	Observed shortwave infrared brightness temperature (K)
X	Predictors in a vertical vector
Y	Predictants in a vertical vector
$\varnothing_Y$	Shortwave infrared eigenvectors
δR^N	Background minus observation for SCENTE
δR^C	Background minus observation for CRTM

Data Availability Statement

The CrIS FSR SDR data are downloaded from NOAA CLASS (https://www.class.noaa.gov). The regression coefficients along with a MATLAB reader are available online (http://digital.library.wisc.edu/1793/80382).

Acknowledgments
This work is supported by CIMSS internal funding and GOES-R and JPSS science projects at CIMSS of the National Oceanic and Atmospheric Administration (NA15NES4320001). The views, opinions, and findings contained in this report are those of the authors and should not be construed as an official National Oceanic and Atmospheric Administration's or U.S. Government's position, policy, or decision. The authors thank Dr. Christopher D. Barnet, Dr. Di Di, and Dr. Wenguang Bai for their valuable discussion, comments, and suggestions on this work and the three anonymous reviewers for their very useful comments to improve our paper. Timothy J. Schmit of NOAA NESDIS is thanked for a review of the manuscript. Manuel López-Puertas was supported by the Spanish Ministerio de Ciencia, Innovación y Universidades (MICINN) under Project ESP2017-87143-R and EC FEDER (European Regional Development Fund) funds.

References

Cardinali, C. (2009). Monitoring the observation impact on the short-range forecast. *Quarterly Journal of the Royal Meteorological Society*, *135*(638), 239–250. https://doi.org/10.1002/qj.366

Chen, Y., Han, Y., van Delst, P., & Weng, F. (2013). Assessment of shortwave infrared sea surface reflection and nonlocal thermodynamic equilibrium effects in the community radiative transfer model using IASI data. *Journal of Atmospheric and Oceanic Technology*, *30*(9), 2152–2160. https://doi.org/10.1175/JTECH-D-12-00267.1

Chen, Y., Han, Y., & Weng, F. Z. (2012). Comparison of two transmittance algorithms in the community radiative transfer model: Application to AVHRR. *Journal of Geophysical Research*, *117*, D06206. https://doi.org/10.1029/2011JD016656

DeSouza-Machado, S. G., Strow, L. L., Hannon, S. E., Motteler, H. E., López-Puertas, M., Funke, B., & Edwards, D. P. (2007). Fast forward radiative transfer modeling of 4.3 μm nonlocal thermodynamic equilibrium effects for infrared temperature sounders. *Geophysical Research Letters*, *34*, L01802. https://doi.org/10.1029/2006GL026684

Diallo, M., Legras, B., Ray, E., Engel, A., & Añel, J. A. (2017). Global distribution of CO_2 in the upper troposphere and stratosphere. *Atmospheric Chemistry and Physics*, *17*, 3861–3878. https://doi.org/10.5194/acp-17-3861-2017

Ding, S., Yang, P., Weng, F., Liu, Q., Han, Y., Van Delst, P., et al. (2011). Validation of the community radiative transfer model. *Journal of Quantitative Spectroscopy & Radiative Transfer*, *112*(6), 1050–1064. https://doi.org/10.1016/j.jqsrt.2010.11.009

Kalogerakis, K. S., Matsiev, D., Sharma, R. D., & Wintersteiner, P. P. (2016). Resolving the mesospheric nighttime 4.3 μm emission puzzle: Laboratory demonstration of new mechanism for OH(υ) relaxation. *Geophysical Research Letters*, *43*, 8835–8843. https://doi.org/10.1002/2016GL069645

Kumer, J. B. (1977). Theory of the CO_2 4.3-μm aurora and related phenomena. *Journal of Geophysical Research*, *82*(16), 2203–2209. https://doi.org/10.1029/JA082i016p02203

Li, Z., Li, J., Jin, X., Schmit, T. J., Borbas, E. E., & Goldberg, M. D. (2010). An objective methodology for infrared land surface emissivity evaluation. *Journal of Geophysical Research*, *115*(D22). https://doi.org/10.1029/2010jd014249

Li, Z., Li, J., Li, Y., Zhang, Y., Schmit, T. J., Zhou, L., et al. (2012). Determining diurnal variations of land surface emissivity from geostationary satellites. *Journal of Geophysical Research: Atmospheres*, *117*(D23). https://doi.org/10.1029/2012jd018279

Liu, E. H., Collard, A., Bi, L., Tong, M., Jung, J., Johnson, B., et al. (2019). EMC contributions to CRTM development and validation. *JCSDA Quarterly*, *63*, 23–25. https://doi.org/10.25923/c23x-ac34

López-Puertas, M., García-Comas, M., Funke, B., Picard, R. H., Winick, J. R., Wintersteiner, P. P., et al. (2004). Evidence for an OH(υ) excitation mechanism of CO_2 4.3 μm nighttime emission from SABER/TIMED measurements. *Journal of Geophysical Research*, *109*, D09307. https://doi.org/10.1029/2003JD004383

López-Puertas, M. & Taylor, F. W. (2001). *Non-LTE radiative transfer in the atmosphere* (Vol. 3). Oxford, UK: World Scientific Publishing Co. Pte. Ltd.

Matricardi, M., López-Puertas, M., & Funke, B. (2018). Modeling of nonlocal thermodynamic equilibrium effects in the classical and principal component-based version of the RTTOV fast radiative transfer model. *Journal of Geophysical Research: Atmospheres*, *123*, 5741–5761. https://doi.org/10.1029/2018JD028657

Menzel, P. W. (2001). Applications with meteorological satellites, World Meteorological Organization (WMO) (Technical Document No. 1078).

Menzel, W. P., Schmit, T. J., Zhang, P., & Li, J. (2018). Satellite based atmospheric infrared sounder development and applications. *Bulletin of the American Meteorological Society*, *99*(3), 583–603. https://doi.org/10.1175/BAMS-D-16-0293.1

Seaman, C. J., & Miller, S. D. (2013). VIIRS captures aurora motions. *Bulletin of the American Meteorological Society*, *94*(10), 1491–1493. https://doi.org/10.1175/BAMS-D-12-00221.1

Seemann, S. W., Borbas, E. E., Knuteson, R. O., Stephenson, G. R., & Huang, H.-L. (2008). Development of a global infrared land surface emissivity database for application to clear sky sounding retrievals from multi-spectral satellite radiance measurements. *Journal of Applied Meteorology and Climatology*, *47*(1), 108–123. https://doi.org/10.1175/2007JAMC1590.1

Sharma, R. D., Wintersteiner, P. P., & Kalogerakis, K. S. (2015). A new mechanism for OH vibrational relaxation leading to enhanced CO_2 emissions in the nocturnal mesosphere. *Geophysical Research Letters*, *42*, 4639–4647. https://doi.org/10.1002/2015GL063724

Stair, A. T., Ulwick, J. C., Baker, K. D., & Baker, D. J. (1975). Rocketborne observations of atmospheric infrared emissions in the auroral region. In B. M. McCormac (Ed.), *Atmospheres of Earth and the planets*, *A Series of Books on the Recent Developments of Space Science and of General Geophysics and Astrophysics Published in Connection with the Journal Space Science Reviews* (Vol. 51, pp. 335–346). Dordrecht, The Netherlands: Springer.

Susskind, J., Blaisdell, J. M., Iredell, L., & Keita, F. (2011). Improved temperature sounding and quality control methodology using AIRS/AMSU data: The AIRS Science Team Version 5 retrieval algorithm. *IEEE Transactions on Geoscience and Remote Sensing*, *49*(3), 883–907. https://doi.org/10.1109/TGRS.2010.2070508

Taylor, J. K., Revercomb, H., & Tobin, D. (2018). An analysis and correction of polarization induced calibration errors for the Cross-track Infrared Sounder (CrIS) sensor. In *Light, energy and the environment 2018 (E2, FTS, HISE, SOLAR, SSL)*, *OSA Technical Digest*. Washington, DC: Optical Society of America.

Tobin, D., Revercomb, H., Knuteson, R., Taylor, J., Best, F., Borg, L., et al. (2013). Suomi-NPP CrIS radiometric calibration uncertainty. *Journal of Geophysical Research: Atmospheres*, *118*, 10,589–10,600. https://doi.org/10.1002/jgrd.50809

Winick, J. R., Mlynczak, M. G., Wintersteiner, P. P., Martin-Torres, F. J., Picard, R. H., Paxton, L. J., et al. (2004). *Thermospheric infrared radiance response to the April 2002 geomagnetic storm from SABER infrared and GUVI ultraviolet limb data*. Paper presented at Proceedings of the SPIE 5235, Remote Sensing of Clouds and the Atmosphere VIII.

Winick, J. R., Picard, R. H., Sharma, R. D., Joseph, R. A., & Wintersteiner, P. P. (1987). Radiative transfer effects on aurora enhanced 4.3 micron emission. *Advances in Space Research*, *10*(10), 17–21.

Yin, M. (2016). Bias characterization of CrIS shortwave temperature sounding channels using fast NLTE model and GFS forecast field. *Journal of Geophysical Research: Atmospheres*, *121*, 1248–1263. https://doi.org/10.1002/2015JD023876

Zavyalov, V., Esplin, M., Scott, D., Esplin, B., Bingham, G., Hoffman, E., et al. (2013). Noise performance of the CrIS instrument. *Journal of Geophysical Research: Atmospheres*, *118*, 13,108–13,120. https://doi.org/10.1002/2013JD020457